Monthly Notices of the ROYAL ASTRONOMICAL SOCIETY

MNRAS **470,** 126–141 (2017) doi:10.1093/mnras/stx1255
Advance Access publication 2017 May 20

The X-ray properties of Be/X-ray pulsars in quiescence

Sergey S. Tsygankov,[1⋆] Rudy Wijnands,[2] Alexander A. Lutovinov,[3,4] Nathalie Degenaar[5] and Juri Poutanen[1,6,7]

[1]*Tuorla Observatory, Department of Physics and Astronomy, University of Turku, Väisäläntie 20, FI-21500 Piikkiö, Finland*
[2]*Anton Pannekoek Institute of Astronomy, University of Amsterdam, Science Park 904, NL-1098 XH Amsterdam, the Netherlands*
[3]*Space Research Institute of the Russian Academy of Sciences, Profsoyuznaya Str. 84/32, Moscow 117997, Russia*
[4]*Moscow Institute of Physics and Technology, Moscow region, Dolgoprudnyi 141701, Russia*
[5]*Institute of Astronomy, University of Cambridge, Madingley Road, Cambridge CB3 OHA, UK*
[6]*Nordita, KTH Royal Institute of Technology and Stockholm University, Roslagstullsbacken 23, SE-10691 Stockholm, Sweden*
[7]*Kavli Institute for Theoretical Physics, University of California, Santa Barbara, CA 93106, USA*

Accepted 2017 May 17. Received 2017 May 17; in original form 2017 March 14

ABSTRACT

Observations of accreting neutron stars (NSs) with strong magnetic fields can be used not only for studying the accretion flow interaction with the NS magnetospheres, but also for understanding the physical processes inside NSs and for estimating their fundamental parameters. Of particular interest are (i) the interaction of a rotating NS (magnetosphere) with the infalling matter at different accretion rates, and (ii) the theory of deep crustal heating and the influence of a strong magnetic field on this process. Here, we present results of the first systematic investigation of 16 X-ray pulsars with Be optical companions during their quiescent states, based on data from the *Chandra*, *XMM–Newton* and *Swift* observatories. The whole sample of sources can be roughly divided into two distinct groups: (i) relatively bright objects with a luminosity around $\sim 10^{34}$ erg s^{-1} and (hard) power-law spectra, and (ii) fainter ones showing thermal spectra. X-ray pulsations were detected from five objects in group (i) with quite a large pulse fraction of 50–70 per cent. The obtained results are discussed within the framework of the models describing the interaction of the infalling matter with the NS magnetic field and those describing heating and cooling in accreting NSs.

Key words: accretion, accretion discs – scattering – stars: magnetic field – stars: neutron – pulsars: general – X-rays: binaries.

1 INTRODUCTION

Transient X-ray pulsars in binary systems with Be optical companions (BeXRPs) are unique laboratories that allow us to test different theories of the accretion on to the magnetized neutron stars (NSs). This is possible due to an extremely broad dynamical range of X-ray luminosities demonstrated by such systems: from $\sim 10^{32–33}$ erg s^{-1} in quiescence to more than $10^{38–39}$ erg s^{-1} during powerful outbursts.

In general, BeXRPs manifest themselves mainly through transient activity of two types: type I – periodically appearing outbursts (once per binary orbit, during the periastron passage) with an X-ray luminosity of $\lesssim 10^{37}$ erg s^{-1} and duration of 20–30 per cent (i.e. typically about one week) of the orbital period; and type II – giant and rare outbursts (usually once in several years) with the peak luminosity exceeding several times 10^{37}–10^{38} erg s^{-1} and lasting from several weeks to months. A review of the observational properties of BeXRPs can be found in Reig (2011).

The presence of a strong magnetic field in X-ray pulsars determines the main observational properties of these objects. For instance, the maximum observed luminosity may exceed the Eddington limit due to the appearance of accretion columns at the magnetic poles of the NSs (Basko & Sunyaev 1976), making them among the brightest accreting objects on the sky (see e.g. recent works by Bachetti et al. 2014; Mushtukov et al. 2015b; Israel et al. 2017, and references therein). Therefore, the temporal and spectral properties of such systems are very sensitive to the magnetic field strength.

BeXRPs can act as unique laboratories thanks to the quite accurate knowledge of the magnetic field strength of the NSs in a substantial fraction of such systems. This has been achieved through the detection of cyclotron absorption features in the spectra of X-ray pulsars and accurate measurements of their energies. Such features are known in more than two dozens of sources (see the recent review of high-mass X-ray binaries by Walter et al. 2015). Measured values

⋆ E-mail: stsygankov@gmail.com

of the cyclotron energy vary between ∼5 and ∼80 keV, which correspond to the magnetic field strengths on the NS surface ranging from $\sim 5 \times 10^{11}$ to $\sim 8 \times 10^{12}$ G. Typical values of spin periods in such systems range from seconds to hundreds of seconds.

In turn, such strong fields can support a magnetosphere of the order of 10^8–10^9 cm, which in some cases can be significantly larger than the corotation radius. In this case, one can expect a termination of the accretion flow due to the centrifugal forces – the so-called propeller regime (Illarionov & Sunyaev 1975; Stella et al. 1985). At the same time, observations of some BeXRPs in a quiescence contradict these expectations. Particularly, a few sources demonstrate X-ray pulsations at luminosities of 10^{33}–10^{34} erg s^{-1} (Motch et al. 1991; Negueruela et al. 2000; Orlandini et al. 2004; Rutledge et al. 2007; Rothschild et al. 2013; Doroshenko et al. 2014; Reig, Doroshenko & Zezas 2014). In different systems, the nature of these pulsations is likely different. For pulsars with large spin periods (dozens of seconds), the required leakage of matter through the magnetospheric barrier can be achieved via quasi-stable accretion from a cold recombined disc (Tsygankov et al. 2017).

Another possible origin of the NS emission in quiescent BeXRPs is their thermal energy accumulated during accretion episodes. Brown, Bildsten & Rutledge (1998) proposed a model in which the NS core is maintained at temperatures of about 10^8 K by nuclear reactions in the crust that occur when it is compressed by freshly accreted material; so-called deep crustal heating. The resulting thermal emission from the NS at its surface is proportional to the average (over thousands to tens of thousands of years) mass accretion rate $\langle \dot{M} \rangle$ and can be as high as $\sim 6 \times 10^{32}$ erg s^{-1} for $\langle \dot{M} \rangle \simeq 10^{-11}$ M$_\odot$ yr^{-1}. This theory is well supported by observations of a number of X-ray binaries (i.e. those harbouring a low magnetic field NS in low-mass X-ray binaries; LMXBs) in quiescence, although for many systems enhanced neutrino cooling processes in the NS core have to be assumed to explain their low temperatures (see e.g. Brown, Bildsten & Rutledge 1998; Yakovlev & Pethick 2004; Heinke et al. 2009, 2010; Wijnands, Degenaar & Page 2013).

Strong magnetic fields may affect the NS heating and cooling processes during the accretion episodes and between them. In contrast to low magnetic field NSs in LMXBs, the accretion in X-ray pulsars proceeds to a fraction of the NS surface as small as ∼0.01 per cent (Mushtukov et al. 2015a). It is currently unclear how the heating of the NS is affected by such inhomogeneous accretion process. Furthermore, the original NS crust in BeXRPs might not have been fully replaced yet with accreted matter (a so-called hybrid crust) that could cause some of the deep crustal heating reactions to be altered or not even to occur (see e.g. Wijnands et al. 2013). In addition, the presence of a strong magnetic field could cause an anisotropy of the thermal conductivity in the crust and therefore likely an anisotropic surface temperature distribution, that affects the cooling history of the NS (see e.g. Shibanov & Yakovlev 1996; Geppert, Küker & Page 2006; Aguilera, Pons & Miralles 2008). At the moment, no systematic studies of the cooling of NSs with strong magnetic fields has been performed, and therefore only limited information is available (for a discussion see Campana et al. 2001, 2002; Wijnands, Degenaar & Page 2013; Elshamouty, Heinke & Chouinard 2016). BeXRPs are the best objects for such studies because they often exhibit distinct outburst and quiescence episodes.

The aim of this work is to study systematically the timing and spectral properties of X-ray pulsars with Be optical companions in their quiescent states. The obtained results give insights into the problem of the accretion on to magnetized NSs at very low mass accretion rates and the possibility to study cooling of the NSs in such systems.

2 DATA ANALYSIS AND RESULTS

2.1 Observations

This work is based mainly on the data from the *Chandra* observatory acquired in the frame of a specially dedicated observational campaign to study quiescent BeXRPs (PI R. Wijnands, ObsIDs. 14635–14650). Additionally, we used the publicly available data from the *Chandra* (ObsIDs. 1919, 10049) and *XMM–Newton* (ObsIDs. 0505280101, 0506190101, 0302970201) observatories, obtained for two sources – 4U 0115+63 and V 0332+53, as well as the data from the XRT telescope onboard the *Swift* observatory, obtained for 4U 0728−25 in the low state (ObsIDs. 00038005001–00038005004). The sample of 16 sources investigated in this work is presented in Table 1 and contains the information about their pulse and orbital periods, distances, optical companions and cyclotron line energies with the corresponding references. The magnetic field of the NS can be estimated from the cyclotron energy using the simple equation $B_{12} = (1+z)E_{\rm cyc}/11.6$ G, where B_{12} the magnetic field strength in units of 10^{12} G, z is the gravitational redshift and $E_{\rm cyc}$ is the cyclotron line energy in keV. Note that there is a quite large uncertainty for the distance estimations of several sources, especially for 2S 1417−624. In such cases, we used the averaged values for the luminosity calculations, i.e. 9 kpc for XTE 1946+274, 12.5 kpc for GS 1843+00 and 6 kpc for 2S 1417−624.

The *Chandra* observations were performed with the ACIS instrument with typical exposures of 5 ks and the *XMM–Newton* observations with the EPIC cameras, had exposures of about 25–30 ks. The data collected by the ACIS instrument were reduced with the standard software package CIAO 4.7[1] with CALDB v4.6.5. One data set (ObsID. 1919) was taken very early in the *Chandra* mission, and therefore we reprocessed it with the CHANDRA_REPRO tools. We extracted spectra and light curves of the sources from circular regions with 2.5–5 arcsec radii (depending on the source intensity). Background events were obtained from circular regions (with radius of 30 arcsec) offset from the sources position. The source 4U 0728−25 was relatively bright during its observations with *Chandra*, which led to pile-up in the data. It was taken into account in the subsequent analysis according to the CIAO threads,[2] namely, by adding the PILEUP model.

To process the *XMM–Newton* data, we used version 14.0 of the *XMM–Newton Science Analysis System (SAS)*. After the standard pipeline processing, we searched for possible intervals of high background and rejected them. This led to a decrease in the effective exposure time by 50–60 per cent down to ≃ 6–14 ks (see details in Table 2). For the analysis of the EPIC data, we selected events with patterns in the range 0–4 for the pn camera and 0–12 for the two MOS cameras, using a circular region with a radius of 20 arcsec around the source positions. Similar to our *Chandra* analysis, background events were selected from circular regions (with radius of 30 arcsec) offset from the source positions.

The *Swift*/XRT telescope observed practically all our objects many times, but the vast majority of these observations were performed during outburst activity. We found that only observations of 4U 0728–25 are suitable for the purpose of this paper. This source was observed four times in 2008 (three times at the end of July and once in December). The source flux during the July observations (ObsIDs. 00038005001, 00038005002, 00038005003; all done in

[1] http://cxc.harvard.edu/ciao/
[2] http://cxc.harvard.edu/ciao/download/doc/pileup_abc.pdf

Table 1. Sample of the studied BeXRPs.

Source name	Pulse period (s)	Orbital period (d)	Distance (kpc)	Cyclotron line (keV)	Optical companion
4U 0115+63	3.6	24.3[1]	7.0[2]	11.5[3]	B0.2Ve[2]
V 0332+53	4.375	34.25[4]	7.0[5]	28[6]	O8–9Ve[5]
MXB 0656−072	160.4	101.2[7]	3.9[8]	36[9]	O9.7Ve[10]
4U 0728−25	103	34.5[11]	6.1[12]	–	O8–9Ve[12]
RX J0812.4−3114	31.9	81.3[13]	9.2[14]	–	B0.5V-IIIe[14]
GS 0834−430	12.3	105.8[15]	5.0[16]	–	B0–2 V–IIIe[16]
GRO J1008−57	93.8	249.5[17]	5.8[18]	88[19], 75.5[20]	B0e[21]
2S 1417−624	17.6	42.1[22]	(1.4–11.1)[23]	–	B1 Ve[23]
2S 1553−542	9.3	30.6[24]	20[25, 26]	23.5[25]	–
Swift J1626.6−5156	15.377	132.9[27]	10[28]	10[29]	B0Ve[28]
GS 1843+00	29.5	–	(10–15)[30]	20[31]	B0–B2IV–Ve[30]
XTE J1946+274	15.8	169.2[32]	(8–10)[33]	36[34]	B0–B1 IV–Ve[33]
KS 1947+300	18.8	40.4[35]	10[36, 37]	12.5[38]	B0Ve[36]
SAX J2103.5+4545	351	12.7[39]	6.5[40]	–	B0Ve[40]
Cep X-4	66.3	21[41]	3.8[42]	30[43]	B1V–B2Ve[42]
SAX J2239.3+6116	1247	262[44]	4.4[44]	–	(B0–2 V–IIIe)[44]

(1) Cominsky et al. (1978), (2) Negueruela & Okazaki (2001), (3) White, Swank & Holt (1983), (4) Stella et al. (1985), (5) Negueruela et al. (1999), (6) Makishima et al. (1990), (7) Yan et al. (2012), (8) McBride et al. (2006), (9) Heindl et al. (2003), (10) Pakull, Motch & Negueruela (2003), (11) Corbet & Peele (1997), (12) Negueruela et al. (1996), (13) Corbet & Peele (2000), (14) Motch et al. (1997), (15) Wilson et al. (1997), (16) Israel et al. (2000), (17) Kuehnel et al. (2012), (18) Riquelme, Torrejón & Negueruela (2012), (19) Shrader et al. (1999), (20) Yamamoto et al. (2013), (21) Coe et al. (1994), (22) Finger, Wilson & Chakrabarty (1996), (23) Grindlay, Petro & McClintock (1984), (24) Kelley, Rappaport & Ayasli (1983), (25) Tsygankov et al. (2016a), (26) Lutovinov et al. (2016), (27) Baykal et al. (2010), (28) Reig et al. (2011), (29) DeCesar et al. (2013), (30) Israel et al. (2001), (31) Mihara (1995), (32) Wilson et al. (2003), (33) Verrecchia et al. (2002), (34) Heindl et al. (2001), (35) Galloway, Morgan & Levine (2004), (36) Negueruela et al. (2003), (37) Tsygankov & Lutovinov (2005), (38) Fürst et al. (2014), (39) Baykal, Stark & Swank (2000), (40) Reig et al. (2004), (41) McBride et al. (2007), (42) Bonnet-Bidaud & Mouchet (1998), (43) Mihara et al. (1991), (44) in't Zand et al. (2000).

the Photon Counting mode) was approximately constant, therefore we were able to combine them to get a source spectrum with better statistics. The XRT spectra were prepared using the online tools provided by the UK Swift Science Data Centre[3] (Evans et al. 2007, 2009).

All observations were also inspected for the presence of coherent signals – pulsations. Note that the time resolution for the *Chandra*/ACIS data is about 3.2 s, which is insufficient to search for pulsations of short-period pulsars. Moreover the measured count rates from most of our sources are very low and the exposures quite short, which also limits the possibility to detect the pulsations.

To trace the long-term history of our sources and to estimate their average accretion rates, we used data from the *RXTE*/ASM (Bradt, Rothschild & Swank 1993, the 2–10 keV energy band) and *Swift*/BAT monitors (Krimm et al. 2013, the 15–50 keV energy band). For illustration purposes in Fig. 1, we present light curves obtained using the *Swift*/BAT all-sky monitor for all sources except RX J0812.4−3114 and SAX J2239.3+6116, which were not detected in the past 20 yr. The raw light curves were downloaded from the *Swift*/BAT Hard X-ray Transient Monitor webpage[4] and converted to mCrab units assuming a constant count rate from the Crab nebula of 0.22 cts cm^{-2} s^{-1} in the 15–50 keV energy range. Depending on the typical count rate from each source, an averaging interval of 1 or 5 d was chosen. In Fig. 1, the times of the observations used in this work are indicated by a horizontal line with the name of the corresponding observatory. In the cases of 4U 0115+63, V 0332+53, GS 0834−43 and KS 1947+300, the data from *RXTE*/ASM[5] are also shown with grey points to illustrate the sources behaviour prior to the *Swift*/BAT observations. Flux measurements were converted to mCrab units similar to the *Swift*/BAT data assuming a constant count rate from the Crab nebula of 75 cts s^{-1}.

The final spectral and timing analysis for all X-ray instruments was done using the standard tools of the FTOOLS/LHEASOFT 6.17 package. In particular, the spectral data were fitted in the 0.5–10 keV energy band using XSPEC package v.12.7.

For fitting the spectra of each source, we used two models: a power-law model (POWERLAW in XSPEC, PL) and a blackbody one (BBODYRAD in XSPEC, BB). The normalization of the latter gives the size of the emission region for the known distance to a source. In both models, absorption by the interstellar medium was included by using the PHABS model. Due to the low count rates (and hence low statistics) for the majority of sources, it was impossible to constrain the absorption columns in our fits. Therefore, we fixed these at the Galactic interstellar values from Kalberla et al. (2005). We note that for several relatively bright sources, we could determine the absorption values with reasonable accuracy and in all these cases they agreed well with the Galactic interstellar values. To keep our analysis uniform, we fixed the absorption columns for these sources to the Galactic values as well. Finally, taking into account that the vast majority of the spectra had small number of photons we binned them to have at least 1 count per energy bin and fitted them using W-statistic (Wachter, Leach & Kellogg 1979).[6] This is a modification of the C-statistic (Cash 1979) valid if a background spectrum with Poisson statistics has been read in. In spite of application of W-statistics, below we use '*C*-value' notation following the common practice.

[3] http://www.swift.ac.uk/user_objects/
[4] http://swift.gsfc.nasa.gov/results/transients/
[5] http://xte.mit.edu/ASM_lc.html

[6] see XSPEC manual; https://heasarc.gsfc.nasa.gov/xanadu/xspec/manual/XSappendixStatistics.html

Table 2. Spectral parameters.

Source	ObsID	Date (MJD)	Exposure (ks)	$N_{\rm H}$ (10^{22} cm^{-2})	$kT_{\rm bb}$ (keV)	$R_{\rm bb}$ (km)	Γ	Observed flux (0.5–10 keV) (erg s^{-1} cm^{-2})	Unabsorbed flux (0.5–10 keV) (erg s^{-1} cm^{-2})	$L_{0.5-10\ \rm keV}$ (erg s^{-1})	C-value (dof)
4U 0115+63	0505280101[a]	54302.07	13.3	0.86	$0.31^{+0.03}_{-0.02}$	$0.76^{+0.19}_{-0.15}$	–	$2.93^{+0.31}_{-0.40} \times 10^{-14}$	$1.00^{+0.12}_{-0.11} \times 10^{-13}$	$5.86^{+0.72}_{-0.64} \times 10^{32}$	161.7(188)
				0.86	–	–	$3.5^{+0.3}_{-0.3}$	$3.85^{+0.53}_{-0.48} \times 10^{-14}$	$1.95^{+0.34}_{-0.25} \times 10^{-13}$	$1.14^{+0.20}_{-0.15} \times 10^{33}$	171.1(188)
V 0332+53	1919	51913.17	5.1	0.70	$0.38^{+0.09}_{-0.07}$	$0.32^{+0.21}_{-0.12}$	–	$1.93^{+0.51}_{-0.51} \times 10^{-14}$	$4.37^{+1.13}_{-1.05} \times 10^{-14}$	$2.56^{+0.66}_{-0.62} \times 10^{32}$	14.6(12)
				0.70	–	–	$3.2^{+0.7}_{-0.6}$	$2.55^{+0.69}_{-0.72} \times 10^{-14}$	$9.12^{+4.68}_{-2.66} \times 10^{-14}$	$5.35^{+2.75}_{-1.56} \times 10^{32}$	12.7(12)
	0506190101[a]	54506.95	14.2	0.70	$0.43^{+0.05}_{-0.04}$	$0.29^{+0.08}_{-0.06}$	–	$2.88^{+0.41}_{-0.34} \times 10^{-14}$	$5.75^{+0.70}_{-0.74} \times 10^{-14}$	$3.37^{+0.41}_{-0.44} \times 10^{32}$	124.0(155)
				0.70	–	–	$2.7^{+0.3}_{-0.3}$	$3.91^{+0.62}_{-0.52} \times 10^{-14}$	$1.00^{+0.15}_{-0.13} \times 10^{-13}$	$5.86^{+0.87}_{-0.76} \times 10^{32}$	124.0(155)
MXB 0656−072	14635	56278.55	4.6	0.60	$0.97^{+0.04}_{-0.04}$	$0.18^{+0.01}_{-0.01}$	–	$1.78^{+0.11}_{-0.14} \times 10^{-12}$	$2.09^{+0.15}_{-0.14} \times 10^{-12}$	$3.80^{+0.27}_{-0.25} \times 10^{33}$	213.0(284)
				0.60	–	–	$1.2^{+0.1}_{-0.1}$	$2.61^{+0.18}_{-0.15} \times 10^{-12}$	$3.09^{+0.22}_{-0.21} \times 10^{-12}$	$5.62^{+0.40}_{-0.38} \times 10^{33}$	221.5(284)
4U 0728−25	0003800500N[b]	54665.59	17.3	0.54	$1.00^{+0.05}_{-0.04}$	$0.25^{+0.02}_{-0.02}$	–	$1.56^{+0.10}_{-0.08} \times 10^{-12}$	$1.78^{+0.13}_{-0.08} \times 10^{-12}$	$7.91^{+0.57}_{-0.36} \times 10^{33}$	276.4(282)
				0.54	–	–	$1.3^{+0.1}_{-0.1}$	$2.09^{+0.13}_{-0.16} \times 10^{-12}$	$2.51^{+0.12}_{-0.17} \times 10^{-12}$	$1.12^{+0.05}_{-0.07} \times 10^{34}$	239.7(282)
	00038005004[b]	54802.36	2.2	0.54	$1.33^{+0.50}_{-0.29}$	$0.10^{+0.05}_{-0.04}$	–	$7.90^{+3.01}_{-2.68} \times 10^{-13}$	$8.71^{+3.59}_{-2.54} \times 10^{-13}$	$3.88^{+1.60}_{-1.13} \times 10^{33}$	13.3(18)
				0.54	–	–	$0.8^{+0.5}_{-0.5}$	$1.07^{+0.54}_{-0.31} \times 10^{-12}$	$1.20^{+0.42}_{-0.33} \times 10^{-12}$	$5.35^{+1.87}_{-1.47} \times 10^{33}$	11.5(18)
RX J0812.4−3114	14637	56486.52	4.6	0.48	$0.13^{+0.03}_{-0.02}$	10.0[c]	–	$1.92^{+0.55}_{-0.56} \times 10^{-14}$	$1.58^{+0.81}_{-0.61} \times 10^{-13}$	$1.60^{+0.82}_{-0.62} \times 10^{33}$	8.3(18)
				0.48	–	–	$5.6^{+1.1}_{-1.1}$	$2.37^{+0.88}_{-0.37} \times 10^{-14}$	$2.51^{+1.56}_{-1.03} \times 10^{-13}$	$2.54^{+1.58}_{-1.05} \times 10^{33}$	8.5(18)
GS 0834−43	14638	56478.08	4.6	1.00	$1.92^{+4.04}_{-0.72}$	$0.01^{+0.01}_{-0.01}$	–	$8.23^{+6.48}_{-3.63} \times 10^{-14}$	$8.91^{+9.71}_{-4.01} \times 10^{-14}$	$2.67^{+2.90}_{-1.20} \times 10^{32}$	9.4(16)
				1.00	–	–	$0.2^{+0.8}_{-0.8}$	$1.15^{+0.74}_{-0.52} \times 10^{-13}$	$1.23^{+0.91}_{-0.52} \times 10^{-13}$	$3.68^{+2.71}_{-1.56} \times 10^{32}$	9.3(16)
GRO J1008−57	14639	56440.72	4.6	1.40	$1.22^{+0.02}_{-0.02}$	$0.49^{+0.02}_{-0.02}$	–	$1.36^{+0.04}_{-0.04} \times 10^{-11}$	$1.66^{+0.04}_{-0.04} \times 10^{-11}$	$6.68^{+0.16}_{-0.15} \times 10^{34}$	658.2(484)
				1.40	–	–	$1.05^{+0.04}_{-0.04}$	$1.84^{+0.05}_{-0.05} \times 10^{-11}$	$2.34^{+0.05}_{-0.05} \times 10^{-11}$	$9.43^{+0.22}_{-0.21} \times 10^{34}$	450.1(484)
2S 1417−624	14640	56432.32	4.6	1.30	$1.57^{+0.34}_{-0.24}$	$0.05^{+0.01}_{-0.01}$	–	$4.07^{+1.20}_{-0.68} \times 10^{-13}$	$4.68^{+1.08}_{-0.88} \times 10^{-13}$	$2.01^{+0.46}_{-0.38} \times 10^{33}$	80.9(68)
				1.30	–	–	$0.6^{+0.3}_{-0.3}$	$5.43^{+0.99}_{-0.98} \times 10^{-13}$	$6.17^{+1.25}_{-0.92} \times 10^{-13}$	$2.66^{+0.54}_{-0.40} \times 10^{33}$	76.84(68)
2S 1553−542	14641	56389.32	4.6	1.70	$0.66^{+0.65}_{-0.25}$	$0.20^{+0.56}_{-0.14}$	–	$1.18^{+0.49}_{-0.44} \times 10^{-14}$	$2.19^{+1.36}_{-0.93} \times 10^{-14}$	$1.05^{+0.65}_{-0.44} \times 10^{33}$	5.8(3)
				1.70	–	–	$2.4^{+1.8}_{-1.4}$	$1.71^{+1.16}_{-0.99} \times 10^{-14}$	$4.68^{+16.70}_{-2.28} \times 10^{-14}$	$2.24^{+7.99}_{-1.09} \times 10^{33}$	4.8(3)
Swift J1626.6−5156	10049	54897.31	18.2	1.00	$1.20^{+0.04}_{-0.04}$	$0.22^{+0.01}_{-0.01}$	–	$8.94^{+0.37}_{-0.42} \times 10^{-13}$	$1.05^{+0.05}_{-0.05} \times 10^{-12}$	$1.25^{+0.06}_{-0.06} \times 10^{34}$	420.0(359)
				1.00	–	–	$1.05^{+0.07}_{-0.07}$	$1.19^{+0.06}_{-0.07} \times 10^{-12}$	$1.45^{+0.07}_{-0.07} \times 10^{-12}$	$1.73^{+0.08}_{-0.08} \times 10^{34}$	315.9(359)
	14642	56307.97	4.6	1.00	$1.22^{+0.23}_{-0.17}$	$0.10^{+0.03}_{-0.02}$	–	$2.05^{+0.54}_{-0.40} \times 10^{-13}$	$2.40^{+0.55}_{-0.40} \times 10^{-13}$	$2.87^{+0.66}_{-0.48} \times 10^{33}$	53.4(46)
				1.00	–	–	$1.0^{+0.3}_{-0.3}$	$2.91^{+0.85}_{-0.62} \times 10^{-13}$	$3.47^{+0.70}_{-0.58} \times 10^{-13}$	$4.15^{+0.84}_{-0.70} \times 10^{33}$	50.6(46)
GS 1843+00	14644	56452.32	4.6	1.00	$2.20^{+6.80}_{-0.92}$	$0.03^{+0.03}_{-0.03}$	–	$7.71^{+8.50}_{-4.15} \times 10^{-14}$	$8.32^{+7.17}_{-3.53} \times 10^{-14}$	$1.55^{+1.34}_{-0.66} \times 10^{33}$	8.1(7)
				1.00	–	–	$0.2^{+1.1}_{-1.1}$	$9.91^{+6.55}_{-5.79} \times 10^{-14}$	$1.07^{+0.71}_{-0.41} \times 10^{-13}$	$2.00^{+1.32}_{-0.77} \times 10^{33}$	8.6(7)

Table 2 – *continued*

Source	ObsID	Date (MJD)	Exposure (ks)	$N_{\rm H}$ (10^{22} cm^{-2})	$kT_{\rm bb}$ (keV)	$R_{\rm bb}$ (km)	Γ	Observed flux (0.5–10 keV) (erg s^{-1} cm^{-2})	Unabsorbed flux (0.5–10 keV) (erg s^{-1} cm^{-2})	$L_{0.5-10\,\rm keV}$ (erg s^{-1})	C-value (dof)
XTE J1946+274	14646	56363.12	4.6	0.90	$1.11^{+0.09}_{-0.08}$	$0.21^{+0.03}_{-0.02}$	–	$7.02^{+0.88}_{-0.61} \times 10^{-13}$	$8.32^{+0.80}_{-0.73} \times 10^{-13}$	$8.06^{+0.78}_{-0.71} \times 10^{33}$	122.8(148)
				0.90	–	–	$1.1^{+0.2}_{-0.2}$	$9.92^{+1.05}_{-0.85} \times 10^{-13}$	$1.20^{+0.12}_{-0.11} \times 10^{-12}$	$1.16^{+0.11}_{-0.10} \times 10^{34}$	108.0(148)
KS 1947+300	14647	56297.13	4.6	0.90	$1.32^{+0.07}_{-0.06}$	$0.30^{+0.02}_{-0.02}$	–	$2.43^{+0.18}_{-0.13} \times 10^{-12}$	$2.75^{+0.20}_{-0.12} \times 10^{-12}$	$3.29^{+0.24}_{-0.15} \times 10^{34}$	256.7(302)
				0.90	–	–	$0.8^{+0.1}_{-0.1}$	$3.42^{+0.19}_{-0.24} \times 10^{-12}$	$3.89^{+0.28}_{-0.18} \times 10^{-12}$	$4.65^{+0.33}_{-0.21} \times 10^{34}$	241.6(302)
SAX J2103.5+4545	14648	56429.01	4.6	0.66	$0.88^{+0.09}_{-0.08}$	$0.14^{+0.02}_{-0.02}$	–	$2.41^{+0.26}_{-0.30} \times 10^{-13}$	$2.95^{+0.44}_{-0.32} \times 10^{-13}$	$1.49^{+0.22}_{-0.16} \times 10^{33}$	79.9(72)
				0.66	–	–	$1.3^{+0.2}_{-0.2}$	$3.89^{+0.96}_{-0.49} \times 10^{-13}$	$4.79^{+0.71}_{-0.62} \times 10^{-13}$	$2.42^{+0.36}_{-0.31} \times 10^{33}$	75.6(72)
Cep X-4	14649	56344.08	4.4	0.80	$0.88^{+0.08}_{-0.07}$	$0.13^{+0.02}_{-0.02}$	–	$5.60^{+0.72}_{-0.41} \times 10^{-13}$	$7.08^{+0.86}_{-0.62} \times 10^{-13}$	$1.22^{+0.15}_{-0.11} \times 10^{33}$	108.6(153)
				0.80	–	–	$1.4^{+0.2}_{-0.2}$	$8.67^{+0.95}_{-1.33} \times 10^{-13}$	$1.12^{+0.11}_{-0.12} \times 10^{-12}$	$1.94^{+0.19}_{-0.21} \times 10^{33}$	101.0(153)
SAX J2239.3+6116	14650	56361.59	4.6	0.85	$1.62^{+0.43}_{-0.30}$	$0.04^{+0.01}_{-0.01}$	–	$4.01^{+0.91}_{-0.89} \times 10^{-13}$	$4.37^{+1.26}_{-0.98} \times 10^{-13}$	$1.01^{+0.29}_{-0.23} \times 10^{33}$	56.5(83)
				0.85	–	–	$0.4^{+0.3}_{-0.3}$	$5.77^{+1.47}_{-1.28} \times 10^{-13}$	$6.31^{+1.45}_{-1.18} \times 10^{-13}$	$1.46^{+0.34}_{-0.27} \times 10^{33}$	56.4(83)

[a]Observations performed by *XMM–Newton.*

[b]Observations performed by *Swift*/XRT; ObdID. 0003800500N means the sum of 00038005001-00038005003 observations.

[c]1σ upper limit on the blackbody radius in RX J0812.4−3114.

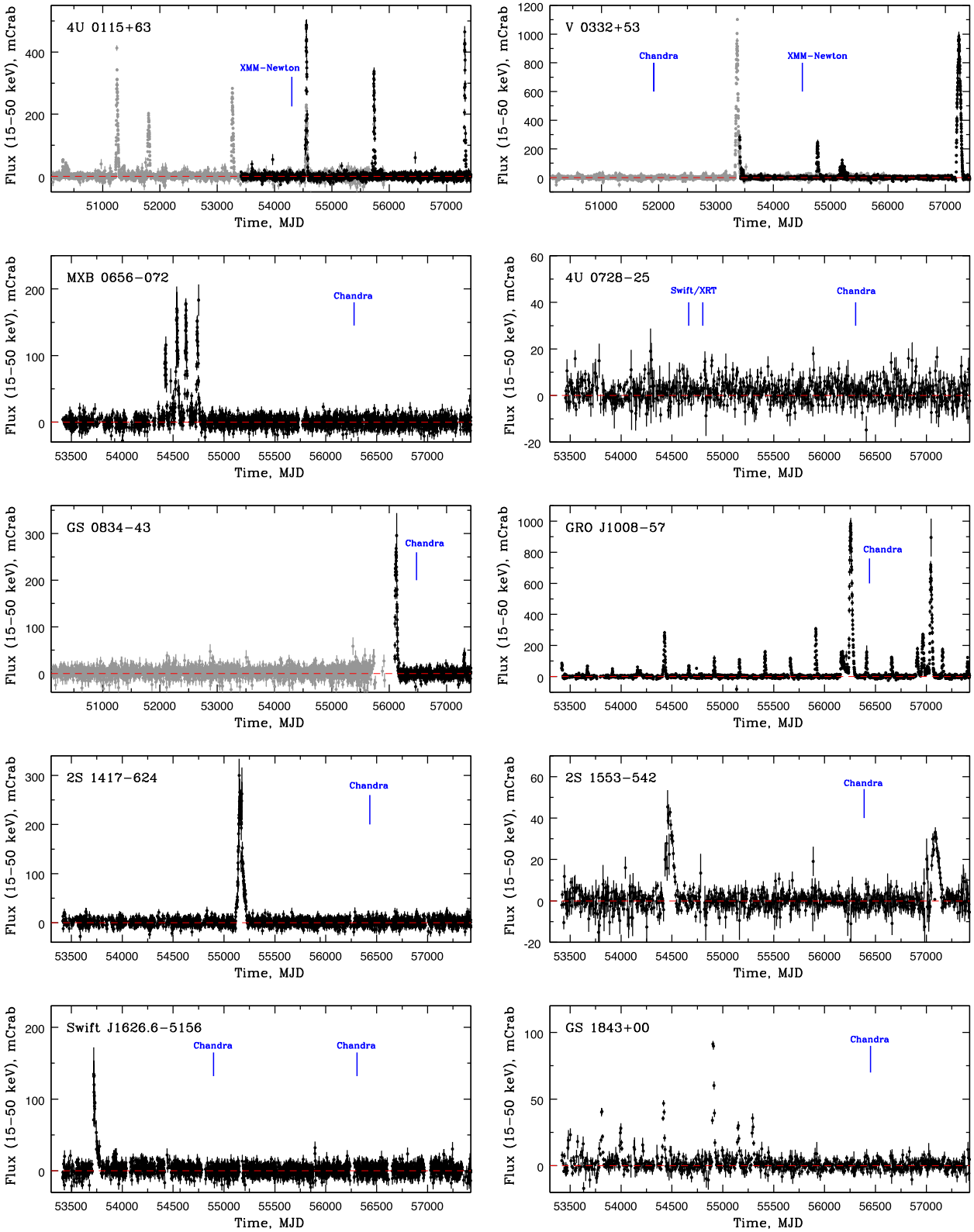

Figure 1. *Swift*/BAT light curves in the 15–50 keV energy range. The times of the *Chandra*, *XMM–Newton* and *Swift*/XRT observations utilized in this work are indicated by the vertical bars. *RXTE*/ASM light curves (grey points) in the 2–10 energy range are shown also for several sources.

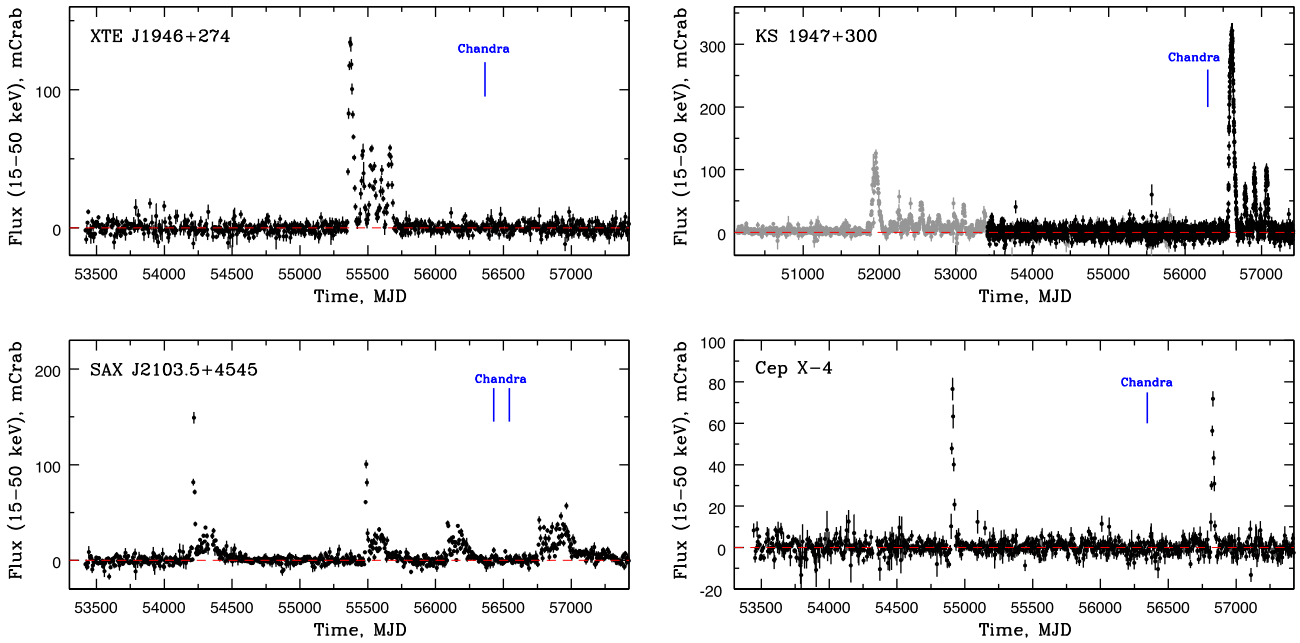

Figure 1 – *continued*

2.2 Spectral analysis

The results of our spectral analysis are summarized in Table 2. The table includes: source name; observation ID (ObsID); start time of the observation (in MJD); effective exposure of the observation; hydrogen column density $N_{\rm H}$, fixed at interstellar one; the blackbody temperature $T_{\rm bb}$ and the radius $R_{\rm bb}$ of the emitting area for the BBODYRAD model and photon index Γ for the POWERLAW model; observed flux in the 0.5–10 keV energy band (note, that it is calculated from the best-fitting model and, therefore is model-dependent); unabsorbed flux in the 0.5–10 keV energy band, calculated using the CFLUX model from the XSPEC package; unabsorbed luminosity in the same energy band; *C*-statistic value for both models and corresponding degrees of freedom (dof). The spectra of our sources are presented in Fig. 2.

Before proceeding to the discussion of the spectral properties of the different sources and groups of them, it is necessary to note that for 4U 0728–25 (ObsID 0003800500N, representing the average of three *Swift*/XRT observations) the start time (Date column) corresponds to the beginning of the observation 00038005001, and the total exposure is the sum of the exposures of observations 00038005001, 00038005002 and 00038005003, which were performed on 2008 July 18, 23 and 25, respectively. Additionally, 4U 0728–25 was observed with the *Chandra* observatory within the framework of our programme (ObsID 14636). In this observation, the source had an unabsorbed luminosity of about 10^{36} erg s^{-1} and a relatively hard X-ray spectrum with a photon index of $\Gamma \simeq 0.5$. Taking into account that this paper is dedicated to the study of BeXRPs at very low luminosities, we excluded this bright observation from our subsequent analysis.

It can be seen from Fig. 3 and Table 2 that for most sources, both spectral models provide a more or less satisfactory fit. To get a quantitative conclusion about the preference of one of the models for a particular source, we used the Akaike information criterion (AIC; Akaike 1974; Burnham, Anderson & Huyvaert 2011) used both in the cosmological tasks (see e.g. Liddle 2007) and to discriminate between different spectral models (see e.g. Sazonov & Khabibullin 2017). In our case, AIC $= 2k + C$, where C is the value from the W-statistics, k is number of model parameters and $k = 2$ for both considered spectral models. The difference $\Delta C = C_{\rm PL} - C_{\rm BB} = 10$ between C-values yielding from two models implies that one of them is $\exp(10/2) \approx 150$ times less probable than the other.

The difference in the C-values for the PL and BB models as a function of the best-fitting power-law index is shown in Fig. 3. It is clearly seen from the figure that $\Delta C = 10$ is reached only for five pulsars where one of the spectral models can be statistically justified over the other one. However, based on the spectral parameters and AIC value, we can roughly divide all sources from our sample into several groups. The first one consists of sources with spectra that are preferentially described by the power-law model: 4U 0728−25, GRO J1008−57, Swift J1626.6−5156, XTE J1946+274, KS 1947+300, *and possibly* GS 0834−43, Cep X-4 and SAX J2239.3+6116. This group harbours the brightest objects from our sample with a luminosity around 10^{34} erg s^{-1}, as well as several fainter systems (down to a few times 10^{33} erg s^{-1}). The typical value of the photon index for these sources is around $\Gamma \sim 1$. The second group includes sources with thermal spectra: 4U 0115+63, V 0332+53 (for both sources the ΔC value is just slightly below 10), and probably RX J0812.4−3114, MXB 0656−072. The temperature of the emission in these systems (using the blackbody model) is $kT \simeq 0.1$–0.4 keV, and the luminosity is very low, a few 10^{32}–10^{33} erg s^{-1}. Note that radii of the emission regions for 4U 0115+63 and V 0332+53 are several hundred metres, which agree well with expected sizes of polar caps of the NS (see e.g. Mushtukov et al. 2015a). Due to very limited statistics, we could not restrict the size of the emission region for RX J0812.4−3114, which has the softest spectrum. A third group includes two sources with a moderate luminosity (2–5) $\times$ 10^{33} erg s^{-1}, for which it is difficult to unambiguously determine their spectral shape: 2S 1417−624 and SAX J2103.5+4545.

We note that SAX J2103.5+4545 was observed with the *Chandra* observatory in 2013 Sep (MJD 56544) with a very long exposure (∼45 ks) in a slightly lower intensity state in comparison to our observations. The source spectrum was well described with an

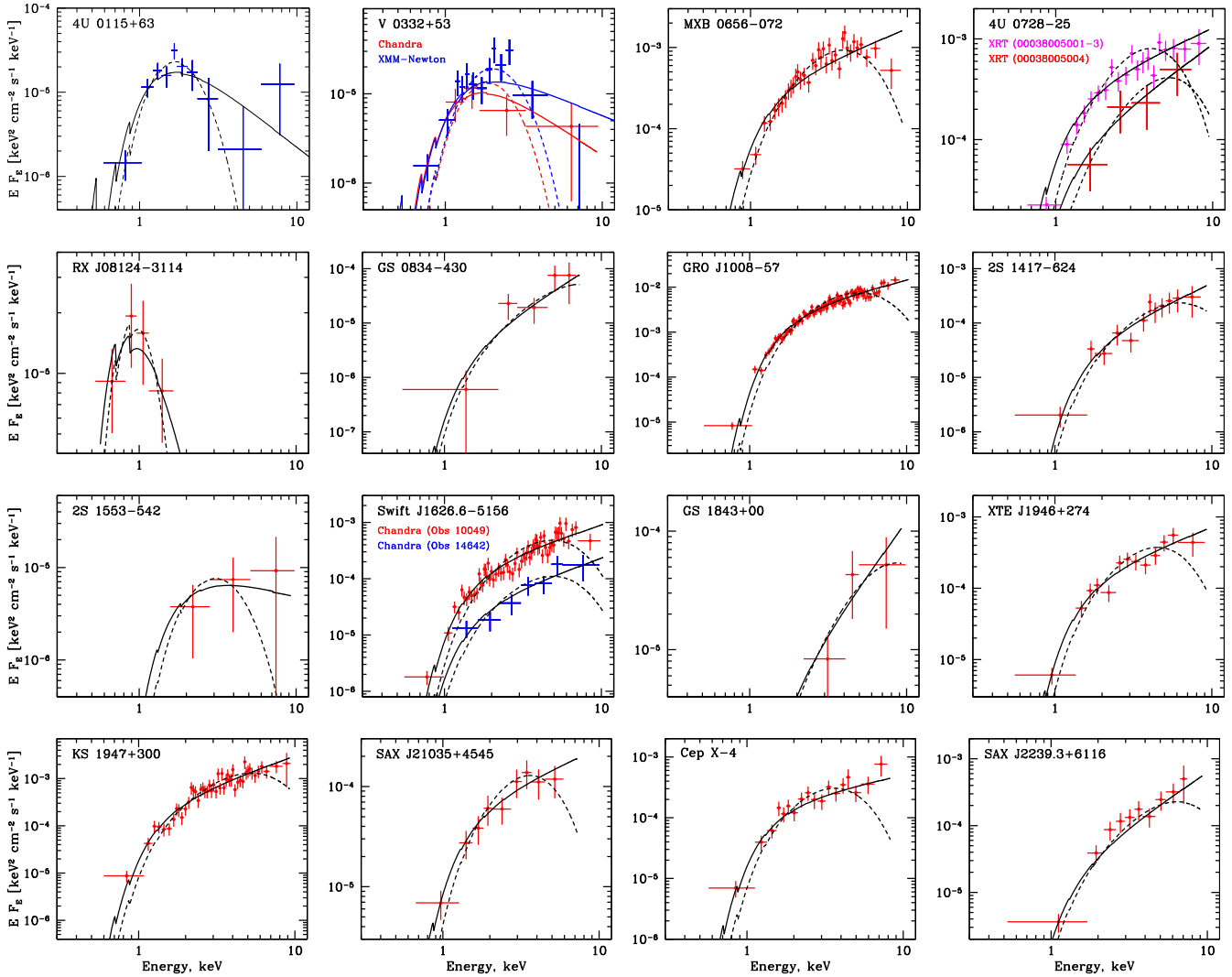

Figure 2. Unfolded X-ray spectra for all the sources in our sample. Solid and dashed lines represent the power-law and blackbody best-fitting models (both modified by absorption), respectively. Data obtained with *Chandra*, *XMM–Newton* and *Swift*/XRT are shown by red circles, blue crosses and magenta squares, respectively, unless stated otherwise.

absorbed blackbody model with a temperature of $kT \simeq 1$ keV and radius of $R = 0.11$ km (Reig et al. 2014), which agrees well with the results of our measurements (Table 2). Therefore, it is likely that also during our observation this source had indeed a spectrum that could be best described by the blackbody model. The count rates for the last two sources – 2S 1553−542 and GS 1843+00 – are extremely low and prevents us from performing detailed spectral analysis inhibiting us from putting them in any of the abovementioned groups.

2.3 Timing analysis

Along with the spectral analysis, we also performed a timing analysis to search for pulsations from all sources in our sample. As a first step all light curves were corrected to the Solar system barycentre. The corrected light curves in the 0.5–10 keV energy range were investigated with the EFSEARCH tool for the presence of a coherent signal. As a result, we detected pulsations from five sources: Swift J1626.6−5156, XTE J1946+274, KS 1946+300, SAX J2103.5+4545 and Cep X-4. For four of them (except SAX J2103.5+4545), pulsations at such low luminosities are detected for the first time. Corresponding pulse profiles are shown in Fig. 4 (zero phase is arbitrary). It is interesting to note that all sources show quite a high pulsed fraction[7] – between 50 and 70 per cent with a characteristic uncertainty of ∼15 per cent. Such high pulsed fraction values are typical for X-ray pulsars both at low accretion rate (see e.g. Lutovinov & Tsygankov 2009) and in the quiescent state (see e.g. Negueruela et al. 2000; Reig et al. 2014). Therefore, it is difficult to make any final conclusions about the origin of the emission in the low state based only on the pulsed fraction value. Very low count statistics and small exposure times did not allow us to put meaningful upper limits on the pulsations presence in the other sources.

3 INDIVIDUAL SOURCES

In this section, we describe the observational properties of each source and compare them with predictions of the relevant

[7] It was determined as $\mathrm{PF} = (F_{\max} - F_{\min})/(F_{\max} + F_{\min})$, where $F_{\max}$ and $F_{\min}$ are the maximum and minimum flux in the pulse profile, respectively.

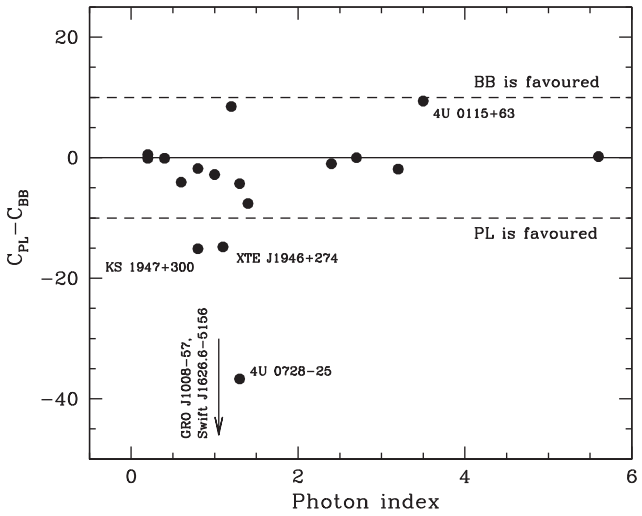

Figure 3. Comparison of the fit quality for the PL and BB models for all sources from our sample. Two horizontal dashed lines indicate the difference $\Delta C = \pm 10$, which may be considered as statistically significant for favouring one of the models over the other. For two sources GRO J1008−57 and Swift J1626.6−5156, $|\Delta C| > 100$, therefore they are indicated by the arrow.

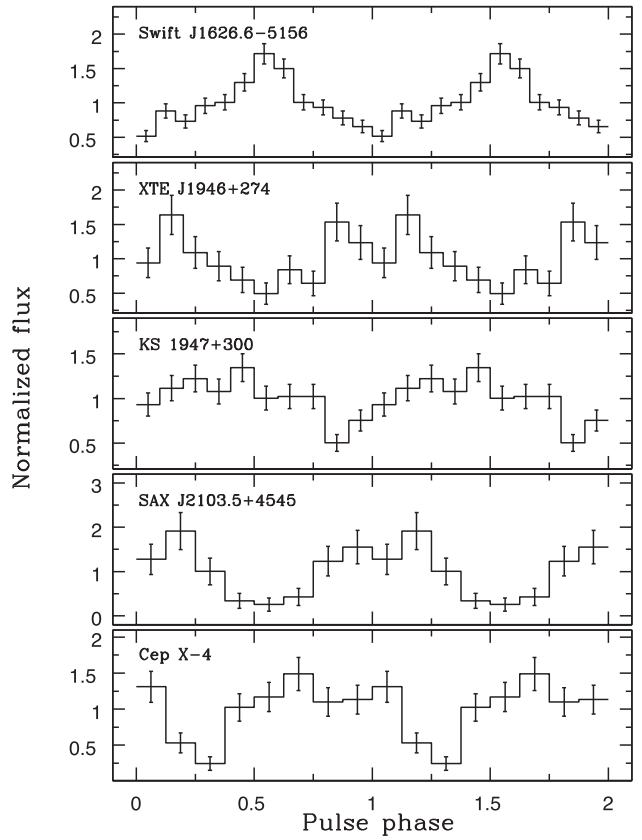

Figure 4. Pulse profiles of five sources with detected pulsations in the 0.5–10 keV energy range.

models presented in Section 4 (the corresponding predictions for the propeller limiting luminosity, averaged mass accretion rate and expected quiescent luminosity are introduced in Section 4 and listed in Table 3). References for the results of previous observations in the quiescent state are presented as well (if available).

3.1 4U 0115+63

XMM–Newton observed 4U 0115+63 about 3 yr after a powerful type II outburst that occurred in 2004 September–October. The source has a thermal spectrum (see Fig. 2) with the temperature of about 0.3 keV and a luminosity around 6×10^{32} erg s^{-1}. This luminosity is a factor of $\sim$10 lower than was observed by the *Swift*/XRT telescope immediately after another giant outburst in 2015 and the subsequent transition of the source to the propeller regime with the typical temperature of 0.5–0.9 keV (Tsygankov et al. 2016c; Wijnands & Degenaar 2016). Our quiescent luminosity is consistent (within the uncertainties) with the one found by Campana et al. (2002) during a BeppoSAX observation of the source.

Due to a long period of a quiescence before the *XMM–Newton* observation, it is quite possible that the crust of the NS was in thermal equilibrium with the core (Rutledge et al. 2002). However, as seen from Fig. 1, the type II outbursts from this source are observed every few years and it is not clear if equilibrium can be achieved on this time-scale. Nevertheless, 4U 0115+63 was observed by *XMM–Newton* with the lowest value of the blackbody temperature.

3.2 V 0332+53

Both *Chandra* and *XMM–Newton* observed V 0332+53 in the very low state. The *Chandra* observation was performed at least 5 yr after any strong outburst activity. However, the period of quiescence could have been much longer, as the *RXTE*/ASM monitor started to operate only in 1996 (before that a bright outburst was observed in 1989). The source spectrum is well fitted with the blackbody model with a temperature of $\sim$0.4 keV and a luminosity $\sim 3 \times 10^{32}$ erg s^{-1}. Similar to 4U 0115+63, this luminosity is a factor of $\sim$10 lower than observed from the heated surface of the NS right after its transition to the propeller regime (Tsygankov et al. 2016c; Wijnands & Degenaar 2016).

Note that during the *XMM–Newton* observation performed about 3 yr after the type II outburst in 2004 Dec to 2005 Jan, the source luminosity and temperature of its blackbody emission were roughly the same as during the *Chandra* observation. Spectral parameters derived in our analysis are consistent within the uncertainties with the results of an independent analysis by Elshamouty et al. (2016) and previous results of Campana et al. (2002).

Our measurements can be used to estimate roughly the characteristic time for the crust to reach thermal equilibrium again with the core (assuming that indeed the accretion of matter during the preceding type-II outburst lifted the crust out of equilibrium). Because the luminosities and temperatures of the source during the *Chandra* and *XMM–Newton* observations were consistent with being the same, we can assume that indeed the NS crust was in equilibrium with the core (else, it is quite likely that after the *XMM–Newton* observation the source would have displayed a hotter crust). Note, that likely the last outburst preceding the *Chandra* observation was detected in 1989, i.e. $\sim$15 yr before. At the same time the *XMM–Newton* observation was performed about 3 yr after the preceding type-II outburst so this would then be an upper limit on the characteristic equilibration time.

3.3 MXB 0656−072

The *Chandra* observation was performed about 4 yr after a sequence of outbursts that started in 2008 October. Based on the above arguments outlined for V 0332+53 on the equilibration time-scale, in MXB 0656−072 the crust may have been in equilibrium with the core at the time of our *Chandra* observation (note this assumes that

Table 3. Determined parameters of the studied BeXRPs.

Source	Period[a] (s)	$L_{\rm prop}(R)$[b] (10^{33} erg s^{-1})	$\langle\dot{M}\rangle$[c] (10^{-10} M$_\odot$ yr^{-1})	$L_{\rm q}$[d] (10^{33} erg s^{-1})	$L_{\rm bb}$[e] (10^{33} erg s^{-1})	$L_{\rm pl}$[f] (10^{33} erg s^{-1})
4U 0115+63	–	174	0.7	4.3	$0.59^{+0.07}_{-0.06}$	$1.14^{+0.20}_{-0.15}$
V 0332+53	–	991	1.0	5.5	$0.26^{+0.07}_{-0.06}$	$0.54^{+0.28}_{-0.16}$
V 0332+53 (XMM)	–	991	1.0	5.5	$0.34^{+0.04}_{-0.04}$	$0.59^{+0.09}_{-0.08}$
MXB 0656−072	–	0.3	0.2	1.3	$3.80^{+0.27}_{-0.25}$	$5.62^{+0.40}_{-0.38}$
4U 0728−25 (XRT aver)	–	[g]	0.2	1.3	$7.91^{+0.57}_{-0.36}$	$11.2^{+0.5}_{-0.7}$
RX J0812.4−3114	–	[g]	0.4	2.2	$1.60^{+0.82}_{-0.62}$	$2.54^{+1.58}_{-1.05}$
GS 0834−430	–	[g]	0.3	1.9	$0.27^{+0.29}_{-0.12}$	$0.37^{+0.27}_{-0.16}$
GRO J1008−57	–	5.5	1.0	5.6	$66.8^{+1.6}_{-1.5}$	$94.3^{+2.2}_{-2.1}$
2S 1417−624	–	[g]	0.3	2.1	$2.01^{+0.46}_{-0.38}$	$2.66^{+0.54}_{-0.40}$
2S 1553−542	–	119	1.5	8.8	$1.05^{+0.65}_{-0.44}$	$2.24^{+7.99}_{-1.09}$
Swift J1626.6−5156 (10049)	15.3360(6)	5.9	0.7	4.3	$12.5^{+0.6}_{-0.6}$	$17.3^{+0.8}_{-0.8}$
Swift J1626.6−5156 (14642)	–	5.9	0.7	4.3	$2.87^{+0.66}_{-0.48}$	$4.15^{+0.84}_{-0.70}$
GS 1843+00	–	5.1	1.2	7.3	$1.55^{+1.34}_{-0.66}$	$2.00^{+1.32}_{-0.77}$
XTE J1946+274	15.760(3)	67	0.3	1.9	$8.06^{+0.78}_{-0.71}$	$11.6^{+1.1}_{-1.0}$
KS 1947+300	18.802(3)	3.7	1.8	10.5	$32.9^{+2.4}_{-1.5}$	$46.5^{+3.3}_{-2.1}$
SAX J21035+4545	350.7(1.1)	[g]	0.5	3.2	$1.49^{+0.22}_{-0.16}$	$2.42^{+0.36}_{-0.31}$
Cep X-4	66.38(3)	1.7	0.05	0.3	$1.22^{+0.15}_{-0.11}$	$1.94^{+0.19}_{-0.21}$
SAX J2239.3+6116	–	[g]	0.06	0.4	$1.01^{+0.29}_{-0.23}$	$1.46^{+0.34}_{-0.27}$

[a]Pulse period, if detected. Uncertainties are quoted at the 1σ level and calculated using the bootstrap approach (for details see Boldin, Tsygankov & Lutovinov 2013).
[b]Propeller limiting luminosity.
[c]Long-term averaged mass accretion rate.
[d]Expected quiescent luminosity in the cooling scenario (using standard core cooling processes).
[e]Unabsorbed luminosity in 0.5–10 keV band assuming a blackbody model.
[f]Unabsorbed luminosity in 0.5–10 keV band assuming a power-law model.
[g]Magnetic field is unknown.

the equilibration time-scale does not vary significantly between the sources). This is supported by the spectral analysis revealing a thermal shape of the spectrum with the blackbody temperature about 1 keV and the luminosity 3.8×10^{33} erg s^{-1}. At the same time, it is about 10 times higher in comparison to the limiting luminosity for the propeller regime onset (see Section 4.1 and Table 3). This discrepancy can be understood in the frame of the cold accretion disc paradigm (see Section 4.2; Tsygankov et al. 2017). Indeed, assuming the same luminosity decline law as obtained in the quoted paper $L \propto t^{-0.7}$, a transition to the cold accretion regime around 10^{35} erg s^{-1}, and absence of transient activity after 2008 outburst, one can expect a luminosity of MXB 0656−072 around a few times 10^{32} erg s^{-1} at the moment of our *Chandra* observation, which is below the observed one. In this case the quiescent luminosity estimated from the deep-crustal heating model ($\sim 1.4 \times 10^{33}$ erg s^{-1} for this pulsar; see Section 4.3) should be the dominant source of emission and naturally explains the soft shape of the energy spectrum.

3.4 4U 0728−25

This source did not exhibit strong outbursts neither in the *RXTE*/ASM nor the *Swift*/BAT data. However, both *Swift*/XRT and *Chandra* observations reveal a bright source with a hard spectrum that is well described by a power-law model. Probably 4U 0728−25 belongs to the class of quasi-persistent sources that never reach a true quiescent state. Also the long spin period of the pulsar makes it a good candidate for accretion from the cold disc. The unknown strength of the magnetic field of the NS in this system makes estimates of the propeller limiting luminosity impossible, which should be much less than the observed luminosity in the case of a standard field.

3.5 RX J0812.4−3114

Bright type II outbursts were never observed from this source, however, a sequence of normal (type I) outbursts occurred in December 1997 (Corbet & Peele 2000). The *RXTE*/ASM and *Swift*/BAT did not detect the source during the whole covered period. The *Chandra* observation revealed a thermal spectrum with a very low temperature of ∼0.1 keV, which is the lowest temperature among our sources. However, the very low counting statistics does not allow us to firmly constrain the spectral parameters of this source. The observed luminosity $\sim 2 \times 10^{33}$ erg s^{-1} agrees with the estimates from the deep-crustal heating model.

3.6 GS 0834−430

The *Chandra* observation utilized in this work was performed slightly less than 1 yr after the bright outburst of this source that occurred in mid-2012. No other significant activity from the source is seen in its light curve starting from 1996 (see Fig. 1). The low number of counts detected from this source does not allow us to discriminate unambiguously between the power-law or blackbody spectral models. However, the quite high blackbody temperature of about 2 keV and small radius of the emitting region hint to a non-thermal origin of the spectrum. At the same time, the observed

luminosity is very low ($\sim 3 \times 10^{32}$ erg s^{-1}). That means that either the crust is not heated at all or the crust cooling time is very short (<1 yr).

3.7 GRO J1008−57

The source was observed with *Chandra* four months after a giant type II outburst and only two weeks after the type I outburst in mid-2013. Both the high source luminosity ($\sim 10^{35}$ erg s^{-1}) and its spectral shape (power law) point to a non-thermal origin of the emission. This conclusion is supported by our recent monitoring of GRO J1008−57 with the *Swift*/XRT that points to the transition of the source to the regime of quasi-stable accretion from the cold disc (Tsygankov et al. 2017).

3.8 2S 1417−624

Chandra observed 2S 1417−624 about 3.3 yr after its bright outburst that occurred in 2009 November. The source spectrum can be equally well fitted with either a power-law or blackbody model with a quite high temperature around 1.5 keV. A long time gap between the outburst and observation would suggests the crust of the NS could have been in the equilibrium with the core. However, then the high observed temperature (when using the blackbody model) is unexpected (unless the cooling indeed originate from very small hot spots of only 50 m in radius; Table 2), pointing to a possibility of continuing accretion on to the NS at a low level. Similar to MXB 0656−072, this accretion can come from the cold disc depleted after 2009 outburst.

3.9 2S 1553−542

This source exhibited only three known outbursts in the history of X-ray observations (in 1975, 2007 and 2015). The *Chandra* data used in this paper were obtained approximately 5 yr after the second outburst in 2007–2008. Taking into account that 2S 1553−542 is the most distance source (20 kpc) in our sample (Lutovinov et al. 2016; Tsygankov et al. 2016a), its counting statistics is very low and prevents us from distinguishing between power-law and blackbody models. However, the temperature obtained using the latter model is ∼0.7 keV, and could point to the thermal origin of the emission that can possibly be attributed to the NS surface emission. The observed luminosity is much lower in comparison to the propeller limiting luminosity supporting this conclusion.

3.10 Swift J1626.6−5156

The source was observed with the *Chandra* observatory twice: 3 and 7 yr after the only bright outburst known for this source (occurring at the beginning of 2006). Both observations show likely a non-thermal spectrum, and no direct crust emission is observed. Despite that the luminosity has dropped by a factor of ∼4 between the two observations, the spectral parameters are very similar and consistent within the uncertainties. It is worth mentioning that the expected limiting luminosity for the transition to the propeller regime is roughly in the middle between the luminosities of these two observations. Such behaviour agrees with the continuous accretion from the cold disc.

Accretion during the brightest observation is supported by the detection of the pulsations with a period of 15.3360(6) s and a pulsed fraction of 54 ± 7 per cent. In the second observation, the pulsations could not be detected and only an upper limit on the pulsed fraction ∼60 per cent was obtained. This limit is consistent with the detected value during the first observation and this non-detection is likely connected with the much shorter exposure of this observation. The pulse period and pulsed fraction values obtained for the first *Chandra* observation are consistent with values published by Içdem, Inam & Baykal (2011) and are typical for this source for periods of its flaring activity (Reig et al. 2008).

3.11 GS 1843+00

The large distance to the source (10–15 kpc) and its low luminosity resulted in very low counting statistics that does not allow us to draw firm conclusions about the nature of the observed emission. The *Chandra* observation was performed around 3 yr after the last outburst detected in the *Swift*/BAT data. The observed luminosity is slightly lower than the propeller limit because the source with such a long spin period likely accretes from the cold disc.

3.12 XTE J1946+274

The source showed a series of strong outbursts in 2011 April. 2 yr later we measured using our *Chandra* data a source luminosity of about 10^{34} erg s^{-1}, which is significantly lower than the expected limiting luminosity for the propeller regime onset (see Table 3). However, we detected a quite hard spectrum (photon index of $\simeq 1.1$) and pulsations suggesting that we observe ongoing accretion on to the NS surface. The spin period was measured to be 15.760(3) s and the pulsed fraction 55 ± 17 per cent typical for the low-luminosity state (see Section 2.3). Our spectral and temporal parameters agree with results of an independent analysis of the same data performed by Özbey Arabacı et al. (2015). The most probable explanation of the hard spectrum of XTE J1946+274 below the propeller line is accretion from the cold disc.

3.13 KS 1947+300

Using *Chandra*, we observed KS 1947+300 about 6 yr after the intense flaring activity seen in 2001–2006 and nine months before another bright outburst in 2013 October (Fig. 1). The source was about 10 times brighter than the expected threshold luminosity for the propeller regime onset and exhibited pulsations with a high pulsed fraction (45 ± 12 per cent). In combination with the hard spectrum this indicates ongoing accretion on to the NS surface probably from the cold disc.

3.14 SAX J2103.5+4545

The source was observed twice with *Chandra* during the same quiescent period (in the middle of 2013 May and September). The results from the second observation were published by Reig et al. (2014) and pointed to the source being in a deep X-ray quiescence. We found similar source flux and spectral parameters in both observations. As mentioned above when describing the spectral fitting, we fixed the absorption at the interstellar value, whereas Reig et al. (2014) determined it from the spectral fitting as $N_{\rm H} = (0.3 \pm 0.1) \times 10^{22}$ cm^{-2}. Fixing the absorption parameter in both observations at this value results in blackbody model parameters that are similar within the errors. We also detected pulsations in the X-ray flux with comparable pulsed fractions of 76 ± 25 and 55 ± 8 per cent for the first and second observations, respectively. It is interesting that a similar high pulsed fraction (although with the different pulse shape) was reported also for this source using an

XMM–Newton observation when the luminosity was three orders of magnitude larger (İnam et al. 2004).

There are at least two ways to explain the observed results: (1) the crust did not heat up much during the previous outburst and the NS crust was already in equilibrium with the core during the first *Chandra* observation and therefore the temperature did not decrease much further when second observation was taken. If indeed cooling emission is observed, then the cooling in this system goes through hot spots (such asymmetric cooling might be possible for the NSs in BeXRPs, see discussion in Wijnands & Degenaar 2016); (2) in the other scenario, we deal with a rather stable low mass accretion rate on the NS surface. In this case, pulsations can be due to accretion on to the magnetic poles, e.g. from the cold disc expected to exist around the NS in this source.

3.15 Cep X-4

The *Chandra* observation was done almost 4 yr after the 2009 March outburst. However, the source exhibited low level flux variability even between major flares explaining the clearly non-thermal spectrum and significantly detected pulsations (pulsed fraction of 70 ± 15 per cent). Most probably the observed power-law luminosity originates from the accretion from the cold disc.

3.16 SAX J2239.3+6116

The source was discovered as a relatively faint transient source and never exhibited strong type II outbursts. The quality of the available data does not allow us to discriminate between the power-law or blackbody spectral models. However, the observed luminosity around 10^{33} erg s^{-1} is typical for BeXRPs in a quiescence and the crust of the NS is likely in the equilibrium with the core. Note that we do not show in Fig. 1 its light curves because the source was not detected in the *Swift*/BAT and *RXTE*/ASM data.

4 DISCUSSION

The observed luminosity in the quiescent state of BeXRPs potentially can be explained with several emission mechanisms or a combination of them: (i) magnetospheric accretion in the propeller regime, (ii) continuing accretion on to the NS from the cold disc, (iii) cooling of the NS surface that is heated due to the accretion of matter when the source was in outburst, (iv) coronal activity of the companion star. Below we discuss those possible explanations of the detected emission and speculate about the role of the NS magnetic field.

4.1 Centrifugal inhibition of accretion

The matter from the accretion disc can be accreted by the NS only if the velocity of the magnetic field lines at the magnetospheric radius is lower than the local Keplerian velocity. Otherwise the pulsar enters the propeller regime and accretion will be inhibited (Illarionov & Sunyaev 1975). An abrupt drop of the luminosity associated with the propeller regime onset was observed in a number of accreting NSs with magnetic fields from 10^8 to 10^{14} G (see, e.g. Revnivtsev & Mereghetti 2015; Tsygankov et al. 2016b; Lutovinov et al. 2017, and references therein).

The threshold value of the accretion luminosity for the onset of the propeller can be roughly estimated by equalising the co-rotation radius R_c to the radius of the magnetosphere R_m (see e.g. Campana et al. 2002)

$$L_{\rm prop}(R) = \frac{GM\dot{M}_{\rm prop}}{R} \simeq 4\times10^{37}k^{7/2}B_{12}^2P^{-7/3}M_{1.4}^{-2/3}R_6^5\ {\rm ergs}^{-1} \quad (1)$$

where P is pulse period in s, $M_{1.4}$ is NS mass in units of 1.4 $M_\odot$, R_6 is NS radius in units of 10^6 cm, B_{12} is magnetic field strength in units of 10^{12} G and k is factor that accounts for the accretion flow geometry ($k \approx 1$ in the case of spherically symmetric accretion and $k \approx 0.5$ in the case of disc accretion; Ghosh & Lamb 1978).

The propeller effect does not permit the matter to penetrate into the magnetosphere and to release its gravitational energy at the NS surface. However, even under such circumstances one can expect to detect an emission originating from the magnetosphere at the radius of R_m (Corbet 1996). Therefore, the maximal luminosity in the propeller regime could be achieved if $R_m = R_c$ (e.g. Campana et al. 2002):

$$L_{\rm prop}(R_c) = \frac{GM\dot{M}_{\rm prop}}{R_c} \simeq 2.4\times10^{35}k^{7/2}B_{12}^2P^{-3}M_{1.4}^{-1}R_6^6\ {\rm ergs}^{-1} \quad (2)$$

A further increase of the mass accretion rate will shrink the magnetosphere inside the co-rotation radius, allowing accretion on to the NS surface to proceed. This will cause a sharp increase of the observed luminosity.

It should be noted that the luminosity estimations done using equation (2) do not take into account the exact spectrum that would arise from the magnetospheric accretion. It was shown by Stella et al. (1994) and Tsygankov et al. (2016c) that for NSs with a strong magnetic field ($\sim10^{12}$ G) the accretion disc is disrupted at large distances and that for a typical mass accretion rate of 10^{16} g s^{-1} one can expect a disc temperature of $\sim$10 eV $\approx 10^5$ K. At such a temperature, the bulk of the radiation should be emitted in the UV band but not in the X-rays.

In contrast to $L_{\rm prop}(R_c)$ the limiting luminosity $L_{\rm prop}(R)$ calculated from equation (1) is not expected to be strongly affected by any systematic biases and can be compared to the observations. The $L_{\rm prop}(R)$ for all sources in our sample that have known distances and magnetic field strengths are listed in Table 3 (assuming disc accretion so that $k = 0.5$). As can be seen, the majority of sources (with exception of MXB 0656−072, GRO J1008−57 and KS 1947+300) emits well below the threshold luminosity $L_{\rm prop}(R)$ for the propeller regime onset. Moreover, for several sources we clearly detected the pulsations (see Table 3) demonstrating the compactness of emitting regions.

The fact that the observed emission level is below the critical one for the propeller regime onset, but the pulsations are still detected, illustrates our poor knowledge of what is going on in this regime. One of possible explanations of the observed properties is a leakage of the matter through the centrifugal barrier. For instance it may happen via a so-called dead accretion disc (Syunyaev & Shakura 1977) as a natural reservoir of the matter around the NS under the condition of the propeller state. If some low-level supply of the matter at the outer radius of the accretion disc continues in the quiescent state, one can expect intermittent or even steady-state penetration of the matter through the centrifugal barrier at the inner disc radius (see e.g. D'Angelo & Spruit 2010, 2012; Zanni & Ferreira 2013). Another explanation proposed recently is a concept of stable accretion from the cold recombined disc around the NS (Tsygankov et al. 2017), which we further explore in the next section.

4.2 Stable accretion from the cold disc

Until recently it was conventionally believed that all X-ray pulsars transit to the propeller regime once their luminosity is dropped to the value $L_{\rm prop}$ determined by equation (1). However, Tsygankov et al. (2017) have shown that such transitions can be observed only in the sources where NSs rotate faster than some critical value for a given magnetic field strength. Otherwise a pulsar will start to accrete stably from a cold recombined accretion disc.

The main idea of the model is that the centrifugal barrier caused by the slowly rotating magnetosphere is strongly suppressed leading to a very low limiting luminosity $L_{\rm prop}$. For a certain combination of the pulsar's spin period and magnetic field strength, this limiting luminosity could be below the one (due to the low-mass accretion rate) that would maintain the temperature throughout the accretion disc above the hydrogen recombination limit of ∼6500 K. Therefore, the hydrogen in the disc would recombine and a cold accretion disc would be formed.

According to the thermal-viscous instability model this would happen in the case when the mass accretion rate drops below some critical value (Lasota 1997):

$$\dot{M} < \dot{M}_{\rm cold} \simeq 3.5 \times 10^{15}\, r_{10}^{2.65}\, M_{1.4}^{-0.88}\, {\rm g\,s^{-1}}, \quad (3)$$

where $r_{10} = r/10^{10}$ cm is the inner disc radius.

For a typical X-ray pulsar with a magnetic field around 2×10^{12} G the corresponding critical luminosity is $L_{\rm cold} \sim 3 \times 10^{34}$ erg s^{-1} (Tsygankov et al. 2017). If during the outburst decay phase this luminosity is reached before the propeller limiting luminosity $L_{\rm prop}$, which is the case for all pulsars with the spin period longer than ∼15 s, the source will stop its fading and will transit to stable accretion from an entirely recombined cold disc.

It is very important to note here that X-ray pulsars that show this transition to accretion from the cold disc will never switch to the propeller regime because of the *decrease* of the inner radius of the disc as the source fades in contrast to accretion from a standard accretion disc where the inner radius is determined by the equation for the magnetospheric radius, i.e. it *increases* as the source fades. If no additional inflow is happening, which is probably true for the BeXRPs in between periastron passages, the luminosity will decrease with time as $L \propto t^{-0.7}$ (Tsygankov et al. 2017). Assuming $L_{\rm cold} \sim 10^{35}$ erg s^{-1} and absence of any mass inflow for a long time (few orbital cycles) then the pulsar can be found at any (low) luminosity.

Presence of the pulsations is expected in the cold disc model because the inner disc radius has always local (effective) temperature around 6500 K, that allows the matter to interact with the magnetic field guiding it to the NS poles. It is worth noting that even the spectral properties cannot give enough information to unambiguously determine whether the emission is of thermal origin or is generated by the low-level accretion. Indeed, as it was discussed by Tsygankov et al. (2016c) the influence of the Comptonization of the X-ray spectrum, originated from the base of the accretion column, by electrons in the optically thin atmosphere is negligible at the accretion luminosity below ∼10^{34}–10^{35} erg s^{-1} because the Thomson optical thickness across the accretion channel is well below unity (Mushtukov et al. 2015a). However, the shape of the initial spectrum depends on the braking distance of the accretion flow, which might be affected by MHD waves, and the opacity in the NS atmosphere. This problem is still under investigation.

4.3 Deep-crustal heating

Another possible source of the emission from quiescent BeXRPs is the surface of the NS that is cooling down after being heated up in the outbursts by the accreted matter. This requires a substantial amount of matter to be accumulated on the NS surface in the course of an outburst. This settling matter compresses the original NS crust and enriches it with low-Z elements (Haensel & Zdunik 1990b). It gives rise to non-equilibrium reactions (electron captures, neutron emissions and pycnonuclear reactions; see e.g. Haensel & Zdunik 1990a, 2003; Gupta et al. 2007; Haensel & Zdunik 2008; Steiner 2012), although the main source of heat generation are the pycnonuclear reactions proceeding deep in the crust at high densities (>10^{12} g cm^{-3}). Most of this heat is conducted inwards to the core, which loses its energy via neutrino emission, but a small part is radiated from the NS surface as thermal photons. This 'deep-crustal heating' (Brown et al. 1998) will slowly heat up the crust. Through this process the long-term averaged mass accretion rate on to the NS is connected to the surface thermal emission (which is a direct probe for the NS core temperature). Particularly, an averaged accretion rate of $\langle\dot{M}\rangle = 10^{-11}$ M$_\odot$ yr^{-1} will provide an averaged thermal NS luminosity at a level of about 6×10^{32} erg s^{-1}.

We note that this assumes that only standard, slow, neutrino cooling processes (e.g. modified Urca, bremsstrahlung) occurring in the core. If fast neutrino cooling (e.g. direct Urca or the neutrino processes that arise if exotic material like mesons, hyperons or unbound quarks are present in the core) occur in the core, then the thermal luminosities from the surface might be significantly reduced (see Brown et al. 1998; Yakovlev & Pethick 2004; Heinke et al. 2009, 2010; Wijnands et al. 2013). However, we note that those enhanced core neutrino processes mostly become active when the NSs are relatively massive (Colpi et al. 2001). Since the NSs in BeXRPs might not have accreted a large amount of matter yet (because of the relatively young age of those systems), it is unclear if indeed enhanced core neutrino processes can be activated in the NSs in BeXRPs.

The averaged mass accretion rate is thus the crucial parameter to estimate the luminosity of the cooling NS predicted by the deep-crustal heating model. Most of the classical BeXRPs spend the majority of their life in quiescence, showing bright outbursts only from time to time. Unfortunately, there is in general no strict recurrence time (except for those that show recurrent type-I outburst every periastron passage) between periods of the activity of Be companions and, hence, the only way to estimate an averaged mass accretion rate is direct observations. In this paper, we used for these estimations data from the *RXTE*/ASM and *SWIFT*/BAT monitors covering together an ∼19 yr time-span (1996–2015). To calculate an averaged flux, we followed the procedure described by Elshamouty et al. (2016). Namely, in the 2–10 keV energy range the averaged count rate obtained from the *RXTE*/ASM data was converted to the flux using the Crab spectrum with standard parameters (photon index of 2.1 and normalization of 10 ph keV^{-1} cm^{-2} s^{-1} at 1 keV), and above 15 keV the flux was derived the same way but using the *Swift*/BAT data. Taking into account difference between spectra of the Crab nebula and typical XRP (we adopted the cut-off power-law model with photon index $\Gamma = 1.0$ and cut-off energy $E_{\rm cut} = 15$ keV; Filippova et al. 2005), the resultant flux must be reduced by ∼30 per cent. We translated it into a luminosity and, consequently, to the mass accretion rate using the simple equation $\langle\dot{M}\rangle = L\,R/G\,M$ (see Table 3). The expected quiescent luminosities from the deep-crustal heating were calculated as $L_{\rm q} = (\langle\dot{M}\rangle/10^{-11}\,{\rm M_\odot\,yr^{-1}}) \times 6 \times 10^{32}$ erg s^{-1} and are presented in the same table. It is worth

noting that due to a very limited history of observations our estimations should be considered as very rough ones with an accuracy not better than an order of magnitude.

Another potential problem is that due to a relatively low sensitivity of the abovementioned all-sky monitors the calculated averaged mass accretion rates are mainly defined by the source fluxes during their outburst activity while the fluxes below the detection threshold are ignored. In the case of the pulsars able to transit to the propeller regime, one may not expect significant heating during quiescence since accretion would be inhibited. However, as it follows from the cold disc model and our analysis, the low-level accretion can still proceed for the sources with relatively long spin periods. Thus, the averaged mass accretion rate estimated using only outbursts activity periods should be treated as a lower limit. However, even if the observed quiescent luminosity in all our sources is due to accretion and always has the same level in quiescence, it will not shift our estimations significantly. For instance, a luminosity of 1×10^{34} erg s^{-1} corresponds to a mass accretion rate of about 9×10^{-13} M$_{\odot}$ yr^{-1}, which is at least two orders of magnitude lower than the values obtained from the all-sky monitors data (see Table 3).

Some pulsars from our sample have observed luminosity L well above predicted $L_{\rm q}$ (e.g. MXB 0656−072, 4U 0728−25, GRO J1008−57, Swift J1626.6−5156, XTE J1946+274, KS 1947+300). Most of these have also hard X-ray spectra and strong X-ray pulsations. Taken together, this suggests that accretion is ongoing in these systems (most probably from the cold disc). Other pulsars, on the other hand, have an observed luminosity that is comparable or lower than the quiescent thermal luminosity predicted to arise from deep crustal heating based on the observed outburst properties (e.g. 4U 0115+63, V 0332+53, RX J0812.4−3114, GS 0834−430, 2S 1417−624, 2S 1553−542, GS 1843+00, SAX J2103.5+4545). The first three of these also exhibit soft thermal spectra. This may suggest that we observe thermal emission from the NS in these objects. For some sources the observed luminosity is significantly lower than predicted from the deep crustal heating model. There could be several reasons for this discrepancy (see also the discussion in Elshamouty et al. (2016) with respect to V 0332+53). We could have significantly overestimated the long-term averaged mass accretion rates. This could happen if the outburst histories of our sources over the past 19 yr are not representative for their activity over the last few millennia (the time-scale that governs the thermal evolution of the core; Colpi et al. 2001; Wijnands et al. 2013). If in the past the sources were less active the averaged accretion rates would be significantly lower and the estimated quiescent luminosities would become more comparable with those observed.

Alternatively, the NS cores could cool significantly faster than assumed in the standard model, potentially indicating the possible presence of enhanced cooling processes in the core. This would require relatively massive NSs (Yakovlev & Pethick 2004). Although some NSs might have been born massive (see the discussion in Elshamouty et al. 2016), it is unclear if this can be true for all of our cooling candidates.

Another possibility is that the heating in the crusts of those sources is less efficient than assumed. As it was discussed by Wijnands et al. (2013) a substantial amount of matter has to be accreted before the original NS crust would be replaced with the new one, that would be enriched with low-Z element. In order to accrete 10^{-4} M$_{\odot}$, the estimated averaged mass accretion rates (see Table 3) have to be constant during $\sim 10^5$–10^7 yr, that is comparable with the lifetime of HMXBs, and therefore some NSs in our sample could have a crust that is not yet fully replaced. It is currently unclear if/how the nuclear heating of such a 'hybrid' crust is different from that of a fully accreted crust (which is assumed in standard heating models, e.g. Haensel & Zdunik 2008). If some of our targets have such a hybrid crust then the deep crustal reactions might be affected and maybe in some sources even inhibited. Consequently, those NSs might not have been heated significantly even if they would accrete currently at a high averaged $\dot{M}$. Since we do not know the exact composition of the NS crust in any system, this adds another uncertainty in our interpretation of the data.

Finally, when fitting the spectra of the thermal sources with a blackbody model, the radii of the emitting regions are very small, much smaller than the NS radius (this is also true if the spectra are fitted with an NS atmosphere model; see Elshamouty et al. 2016). This could indicate that the cooling occurs via hotspots at the magnetic poles (see the discussion in Wijnands & Degenaar 2016). This would cause pulsations in the light curves but the quality of our data does not allow to put constraints on that possibility for those sources. However, as determined by Elshamouty et al. (2016) for V 0332+53, the rest of the NS surface also emits some radiation. Although the temperature of the rest of the surface should be significantly lower than what is observed from the hotspots, the emitting region is much larger and the total luminosity emitted from the rest of the NS surface could be significantly larger than the power emitted from the hotspots. Therefore, the sources could still be consistent with the standard heating and cooling models (see e.g. fig. 3 of Elshamouty et al. 2016). Unfortunately, our current data sets do not allow us to put any constraints on the possible emission from the rest of the surface. However, this potential contribution has to be taken into account when modelling the cooling emission from high-magnetic field NSs.

Besides that we might directly probe the NS cores for our cooling candidates, it is possible that during some outbursts (i.e. the giant outbursts) enough heat was generated in the crust so that the crust departed from thermal equilibrium with the core. In such cases, the thermal luminosity would represent the thermal state of the crust and not that of the core and potentially we could observe (using multiple observations of the same source) the crust cooling until equilibrium is restored (see Wijnands & Degenaar 2016, for this possibility). The source GS 0834−430 was observed within 1 yr after its type-II outburst in 2012 at a rather low luminosity of 3×10^{32} erg s^{-1}. This low luminosity would indicate that the crust was already in thermal equilibrium with the core during the time of our observation, unless the core is very cold. If truly in equilibrium, this would constrain the crust cooling time-scale to be less than 1 yr. This is consistent with what is reported by Rouco Escorial et al. (2017) who found a crust cooling time-scale of less than 250 d for 4U 0115+63. All the other sources in our sample were observed much longer after their last giant outbursts. Despite that it is not clear that the crust cooling time-scales in all NSs should be of the same duration, it is plausible that for all our cooling candidates, the crust was in equilibrium with the core during the time of our observations.

4.4 Contamination from the optical counterpart

The majority of previous studies dedicated to the thermal emission of NSs in the quiescent state were based on observations of LMXBs. However, in contrast to LMXBs, BeXRPs harbour massive and hot optical companions of O and B classes, which are known to emit some non-negligible fraction of their bolometric luminosity in X-rays (Cassinelli & Olson 1979; Seward et al. 1979).

Systematic studies of X-ray properties of O and B stars have been done using different observatories (see e.g. Berghoefer et al. 1997 for the *ROSAT* data, Nazé 2009 for the *XMM–Newton* data, Nazé et al. 2011 for the *Chandra* data, and references therein).

Particularly, it was shown that spectra of O stars can be well fitted by a blackbody model with a temperature between ∼0.2 and ∼0.6 keV with additional absorption above the interstellar one. The B stars have harder spectra with temperatures around 1 keV and usually do not require additional local absorption.

The X-ray luminosity of O stars clearly correlates with the bolometric one, whereas for B stars such a correlation is not obvious and has a large scatter. Besides the intrinsic scatter, some additional one can be introduced by the magnetic field of the star and its binary nature (particularly, due to an interaction of the emission from the compact object with the stellar wind).

Using fig. 3 from Nazé et al. (2011), we can roughly estimate the expected X-ray luminosities for the optical companions of the pulsars in our sample. As can be seen from Table 1, the spectral types of companions cover a relatively narrow range from O8 to B2. According to the abovementioned paper, such stars emit around 10^{-7} of their bolometric luminosity in the X-rays, which makes several times 10^{31} erg s^{-1}. This value is about two orders of magnitude lower than the luminosity measured in our observations for the majority of sources. The lowest luminosities are demonstrated by 4U 0115+63 and V 0332+53 and, at the same time, those systems are amongst the one with the hottest optical companions. Therefore, these sources are the only objects from the sample where some contribution from the optical star may be present but it is not expected to be significant.

5 CONCLUSIONS

In this work, we presented results of the first systematic survey of the sample of 16 X-ray pulsars with Be optical companions during quiescent state. The observations were taken with the *Chandra*, *XMM–Newton* and *Swift* observatories with different delays after an outburst activity of the sources. This gave us a possibility to study thermal evolution of highly magnetized NSs in details. Surprisingly, a substantial fraction of the sources from our sample have hard energy spectra even at low luminosities implying continuing accretion. Five of them show strong pulsations with pulse fraction of 50–70 per cent. Such behaviour can be explained in terms of the recently proposed model of stable accretion from the cold disc (Tsygankov et al. 2017). For the rapidly rotating pulsars that are able to transit to the propeller regime much softer spectra were observed. Measured blackbody temperature and very low luminosity indicate cooling process of the NS heated up in the outbursts by the accreted matter. The obtained results were discussed within the framework of the 'deep-crustal heating' model (Brown et al. 1998).

To make more strict conclusions on the cooling processes in the magnetized NSs, deeper multiple observations of the pulsars in their quiescent state are needed. Additionally, to be able to robustly discriminate thermal spectra from the non-thermal ones, very deep observations should be performed with instruments possessing a high sensitivity in a broad energy range, e.g. the *NuSTAR* observatory. Furthermore, such observations should be performed only for the sources that are able to transit to the propeller regime, i.e. rotating rapidly enough to centrifugally halt the accretion before the disc transits to the fully recombined state (Tsygankov et al. 2017).

ACKNOWLEDGEMENTS

We thank Alexander Mushtukov and Valery Suleimanov for helpful discussions. This work made use of the *Chandra* and *XMM–Newton* public data archives as well as data of *Swift* supplied by the UK Swift Science Data Centre at the University of Leicester. AAL and SST acknowledge support by the Russian Science Foundation grant 14-12-01287 in part of the individual sources analysis and theoretical discussions (Sections 3 and 4). AAL also thanks the Dynasty Foundation for its support in analysing the X-ray data (Section 2). RW is supported by an NWO Top Grant, Module 1. ND acknowledges support via an NWO/Vidi grant and an EU Marie Curie Intra-European fellowship under contract no. FP-PEOPLE-2013-IEF-627148. JP was partially supported by the Academy of Finland grant 268740 and the National Science Foundation grant PHY-1125915.

REFERENCES

Aguilera D. N., Pons J. A., Miralles J. A., 2008, ApJ, 673, L167
Akaike H., 1974, IEEE Trans. Autom. Control, 19, 716
Bachetti M. et al., 2014, Nature, 514, 202
Basko M. M., Sunyaev R. A., 1976, MNRAS, 175, 395
Baykal A., Stark M. J., Swank J., 2000, ApJ, 544, L129
Baykal A., Göğüş E., İnam S. Ç., Belloni T., 2010, ApJ, 711, 1306
Berghoefer T. W., Schmitt J. H. M. M., Danner R., Cassinelli J. P., 1997, A&A, 322, 167
Boldin P. A., Tsygankov S. S., Lutovinov A. A., 2013, Astron. Lett., 39, 375
Bonnet-Bidaud J. M., Mouchet M., 1998, A&A, 332, L9
Bradt H. V., Rothschild R. E., Swank J. H., 1993, A&AS, 97, 355
Brown E. F., Bildsten L., Rutledge R. E., 1998, ApJ, 504, L95
Burnham K. P., Anderson D. R., Huyvaert K. P., 2011, Behav. Ecol. Sociobiol., 65, 23
Campana S., Gastaldello F., Stella L., Israel G. L., Colpi M., Pizzolato F., Orlandini M., Dal Fiume D., 2001, ApJ, 561, 924
Campana S., Stella L., Israel G. L., Moretti A., Parmar A. N., Orlandini M., 2002, ApJ, 580, 389
Cash W., 1979, ApJ, 228, 939
Cassinelli J. P., Olson G. L., 1979, ApJ, 229, 304
Coe M. J. et al., 1994, MNRAS, 270, L57
Colpi M., Geppert U., Page D., Possenti A., 2001, ApJ, 548, L175
Cominsky L., Clark G. W., Li F., Mayer W., Rappaport S., 1978, Nature, 273, 367
Corbet R. H. D., 1996, ApJ, 457, L31
Corbet R. H. D., Peele A. G., 1997, ApJ, 489, L83
Corbet R. H. D., Peele A. G., 2000, ApJ, 530, L33
D'Angelo C. R., Spruit H. C., 2010, MNRAS, 406, 1208
D'Angelo C. R., Spruit H. C., 2012, MNRAS, 420, 416
DeCesar M. E., Boyd P. T., Pottschmidt K., Wilms J., Suchy S., Miller M. C., 2013, ApJ, 762, 61
Doroshenko V., Santangelo A., Doroshenko R., Caballero I., Tsygankov S., Rothschild R., 2014, A&A, 561, A96
Elshamouty K. G., Heinke C. O., Chouinard R., 2016, MNRAS, 463, 78
Evans P. A. et al., 2007, A&A, 469, 379
Evans P. A. et al., 2009, MNRAS, 397, 1177
Filippova E. V., Tsygankov S. S., Lutovinov A. A., Sunyaev R. A., 2005, Astron. Lett., 31, 729
Finger M. H., Wilson R. B., Chakrabarty D., 1996, A&AS, 120, 209
Fürst F. et al., 2014, ApJ, 784, L40
Galloway D. K., Morgan E. H., Levine A. M., 2004, ApJ, 613, 1164
Geppert U., Küker M., Page D., 2006, A&A, 457, 937
Ghosh P., Lamb F. K., 1978, ApJ, 223, L83
Grindlay J. E., Petro L. D., McClintock J. E., 1984, ApJ, 276, 621
Gupta S., Brown E. F., Schatz H., Möller P., Kratz K.-L., 2007, ApJ, 662, 1188
Haensel P., Zdunik J. L., 1990a, A&A, 227, 431
Haensel P., Zdunik J. L., 1990b, A&A, 229, 117
Haensel P., Zdunik J. L., 2003, A&A, 404, L33
Haensel P., Zdunik J. L., 2008, A&A, 480, 459
Heindl W. A., Coburn W., Gruber D. E., Rothschild R. E., Kreykenbohm I., Wilms J., Staubert R., 2001, ApJ, 563, L35

Heindl W., Coburn W., Kreykenbohm I., Wilms J., 2003, Astron. Telegram, 200
Heinke C. O., Jonker P. G., Wijnands R., Deloye C. J., Taam R. E., 2009, ApJ, 691, 1035
Heinke C. O. et al., 2010, ApJ, 714, 894
Içdem B., Inam S., Baykal A., 2011, MNRAS, 415, 1523
Illarionov A. F., Sunyaev R. A., 1975, A&A, 39, 185
İnam S. Ç., Baykal A., Swank J., Stark M. J., 2004, ApJ, 616, 463
in't Zand J. J. M., Halpern J., Eracleous M., McCollough M., Augusteijn T., Remillard R. A., Heise J., 2000, A&A, 361, 85
Israel G. L. et al., 2000, MNRAS, 314, 87
Israel G. L. et al., 2001, A&A, 371, 1018
Israel G. L. et al., 2017, Science, 355, 817
Kalberla P. M. W., Burton W. B., Hartmann D., Arnal E. M., Bajaja E., Morras R., Pöppel W. G. L., 2005, A&A, 440, 775
Kelley R. L., Rappaport S., Ayasli S., 1983, ApJ, 274, 765
Krimm H. A. et al., 2013, ApJS, 209, 14
Kuehnel M. et al., 2012, Astron. Telegram, 4564
Lasota J. P., 1997, in Wickramasinghe D. T., Bicknell G. V., Ferrario L., eds, ASP Conf. Ser. Vol. 121, Proc. IAU Colloq. 163: Accretion Phenomena and Related Outflows. Astron. Soc. Pac., San Francisco, p. 351
Liddle A. R., 2007, MNRAS, 377, L74
Lutovinov A. A., Tsygankov S. S., 2009, Astron. Lett., 35, 433
Lutovinov A. A., Buckley D. A. H., Townsend L. J., Tsygankov S. S., Kennea J., 2016, MNRAS, 462, 3823
Lutovinov A. A., Tsygankov S. S., Krivonos R. A., Molkov S. V., Poutanen J., 2017, ApJ, 834, 209
McBride V. A. et al., 2006, A&A, 451, 267
McBride V. A. et al., 2007, MNRAS, 382, 743
Makishima K. et al., 1990, ApJ, 365, L59
Mihara T., 1995, PhD thesis, Univ. Tokyo
Mihara T., Makishima K., Kamijo S., Ohashi T., Nagase F., Tanaka Y., Koyama K., 1991, ApJ, 379, L61
Motch C., Stella L., Janot-Pacheco E., Mouchet M., 1991, ApJ, 369, 490
Motch C., Haberl F., Dennerl K., Pakull M., Janot-Pacheco E., 1997, A&A, 323, 853
Mushtukov A. A., Suleimanov V. F., Tsygankov S. S., Poutanen J., 2015a, MNRAS, 447, 1847
Mushtukov A. A., Suleimanov V. F., Tsygankov S. S., Poutanen J., 2015b, MNRAS, 454, 2539
Nazé Y., 2009, A&A, 506, 1055
Nazé Y. et al., 2011, ApJS, 194, 7
Negueruela I., Okazaki A. T., 2001, A&A, 369, 108
Negueruela I., Roche P., Buckley D. A. H., Chakrabarty D., Coe M. J., Fabregat J., Reig P., 1996, A&A, 315, 160
Negueruela I., Roche P., Fabregat J., Coe M. J., 1999, MNRAS, 307, 695
Negueruela I., Reig P., Finger M. H., Roche P., 2000, A&A, 356, 1003
Negueruela I., Israel G. L., Marco A., Norton A. J., Speziali R., 2003, A&A, 397, 739
Orlandini M. et al., 2004, Nucl. Phys. B, 132, 476
Özbey Arabacı M. et al., 2015, A&A, 582, A53
Pakull M. W., Motch C., Negueruela I., 2003, Astron. Telegram, 202
Reig P., 2011, Ap&SS, 332, 1
Reig P., Negueruela I., Fabregat J., Chato R., Blay P., Mavromatakis F., 2004, A&A, 421, 673
Reig P., Belloni T., Israel G. L., Campana S., Gehrels N., Homan J., 2008, A&A, 485, 797
Reig P., Nespoli E., Fabregat J., Mennickent R. E., 2011, A&A, 533, A23
Reig P., Doroshenko V., Zezas A., 2014, MNRAS, 445, 1314
Revnivtsev M., Mereghetti S., 2015, Space Sci. Rev., 191, 293
Riquelme M. S., Torrejón J. M., Negueruela I., 2012, A&A, 539, A114
Rothschild R. et al., 2013, ApJ, 770, 19
Rouco Escorial A., Bak Nielsen A. S., Wijnands R., Cavecchi Y., Degenaar N., Patruno A., 2017, MNRAS, in press
Rutledge R. E., Bildsten L., Brown E. F., Pavlov G. G., Zavlin V. E., Ushomirsky G., 2002, ApJ, 580, 413
Rutledge R. E., Bildsten L., Brown E. F., Chakrabarty D., Pavlov G. G., Zavlin V. E., 2007, ApJ, 658, 514
Sazonov S., Khabibullin I., 2017, MNRAS, 466, 1019
Seward F. D., Forman W. R., Giacconi R., Griffiths R. E., Harnden F. R., Jr, Jones C., Pye J. P., 1979, ApJ, 234, L55
Shibanov Y. A., Yakovlev D. G., 1996, A&A, 309, 171
Shrader C. R., Sutaria F. K., Singh K. P., Macomb D. J., 1999, ApJ, 512, 920
Steiner A. W., 2012, Phys. Rev. C, 85, 055804
Stella L., White N. E., Davelaar J., Parmar A. N., Blissett R. J., van der Klis M., 1985, ApJ, 288, L45
Stella L., Campana S., Colpi M., Mereghetti S., Tavani M., 1994, ApJ, 423, L47
Syunyaev R. A., Shakura N. I., 1977, Sov. Astron. Lett., 3, 138
Tsygankov S. S., Lutovinov A. A., 2005, Astron. Lett., 31, 88
Tsygankov S. S., Lutovinov A. A., Krivonos R. A., Molkov S. V., Jenke P. J., Finger M. H., Poutanen J., 2016a, MNRAS, 457, 258
Tsygankov S. S., Mushtukov A. A., Suleimanov V. F., Poutanen J., 2016b, MNRAS, 457, 1101
Tsygankov S. S., Lutovinov A. A., Doroshenko V., Mushtukov A. A., Suleimanov V., Poutanen J., 2016c, A&A, 593, A16
Tsygankov S. S., Mushtukov A. A., Suleimanov V. F., Doroshenko V., Lutovinov A. A., Poutanen J., 2017, A&A, preprint (arXiv:1703.04528)
Verrecchia F. et al., 2002, A&A, 393, 983
Wachter K., Leach R., Kellogg E., 1979, ApJ, 230, 274
Walter R., Lutovinov A. A., Bozzo E., Tsygankov S. S., 2015, A&AR, 23, 2
White N. E., Swank J. H., Holt S. S., 1983, ApJ, 270, 711
Wijnands R., Degenaar N., 2016, MNRAS, 463, L46
Wijnands R., Degenaar N., Page D., 2013, MNRAS, 432, 2366
Wilson C. A., Finger M. H., Harmon B. A., Scott D. M., Wilson R. B., Bildsten L., Chakrabarty D., Prince T. A., 1997, ApJ, 479, 388
Wilson C. A., Finger M. H., Coe M. J., Negueruela I., 2003, ApJ, 584, 996
Yakovlev D. G., Pethick C. J., 2004, ARA&A, 42, 169
Yamamoto T., Mihara T., Sugizaki M., Sasano M., Makishima K., Nakajima M., 2013, Astron. Telegram, 4759
Yan J., Zurita Heras J. A., Chaty S., Li H., Liu Q., 2012, ApJ, 753, 73
Zanni C., Ferreira J., 2013, A&A, 550, A99

This paper has been typeset from a TEX/LATEX file prepared by the author.